AGU PUBLICATIONS

Geophysical Research Letters

RESEARCH LETTER
10.1002/2017GL076223

Key Points:
- Phase match filtering detects new seismic events describing in detail the seismicity pattern before the $M_w = 6.0$, 2016 Amatrice earthquake
- Variations in the release rate of the seismic activity along a midcrustal shear zone may represent a signature of tectonic loading
- The seismicity pattern along a midcrustal shear zone suggests stress transfer in the upper crust favoring the unlocking of the main fault

Supporting Information:
- Supporting Information S1

Correspondence to:
A. Vuan,
avuan@inogs.it

Citation:
Vuan, A., Sugan, M., Chiaraluce, L., & Di Stefano, R. (2017). Loading rate variations along a midcrustal shear zone preceding the M_w6.0 earthquake of 24 August 2016 in Central Italy. *Geophysical Research Letters*, *44*, 12,170–12,180. https://doi.org/10.1002/2017GL076223

Received 31 JUL 2017
Accepted 26 NOV 2017
Accepted article online 1 DEC 2017
Published online 26 DEC 2017

Loading Rate Variations Along a Midcrustal Shear Zone Preceding the M_w6.0 Earthquake of 24 August 2016 in Central Italy

A. Vuan[1], M. Sugan[1], L. Chiaraluce[2], and R. Di Stefano[2]

[1]OGS, Istituto Nazionale di Oceanografia e di Geofisica Sperimentale, Trieste, Italy, [2]INGV, Istituto Nazionale di Geofisica e Vulcanologia, Rome, Italy

Abstract To identify greater detail in the seismicity pattern preceding the 24 August 2016 M_w6.0 earthquake in Central Italy, we apply waveform matching using 1,028 events as templates. In the 8 months before the mainshock, we find ~2,000 additional earthquakes mostly located along a subhorizontal shear zone (SZ) bounding at depth the extensional fault system. Asynchrony is observed in the occurrence of events nucleating along the SZ compared to the ones on fault portions embedded in the shallower upper crust, with the former anticipating the latter. Within the SZ, we also observe along-strike seismic migration episodes with earthquakes pointing toward the M_w6.0 mainshock nucleation zone. These episodes are followed by an apparent quiescence within the main fault area. We suggest that the variations in the seismic activity along the SZ represent the brittle signature of the tectonic loading process enabling portions of the overlaying normal faults to become unlocked.

1. Introduction

The observation of deformation mechanisms active at upper and midcrustal depths together with the measurement of physical properties variations of fault zones materials is essential to our understanding of fault loading processes, earthquake physics, and the preparatory phase for faults embedded in the continental crust. Early theoretical models based on geological studies of exhumed faults proposed a localized fault zone of elastofrictional behavior overlying regions where quasi-plastic processes occur along shear zones (Sibson, 1977). Later on, laboratory data were used to propose models for fault rheology where a brittle upper crust with faults strength obeying Byerlee's friction rules (Byerlee, 1978) overlies more ductile portions where fault behavior is plastic due to increasing temperature (Brace & Kohlstedt, 1980). Such models are essentially coherent with the earthquake distribution at depth showing the role of brittle-ductile transition zones separating a seismogenic upper crust deforming via pressure-dependent and temperature-insensitive brittle frictional sliding and an aseismic lower crust deforming via temperature-dependent and pressure-insensitive ductile processes such as dislocation creep (Sibson, 1982). Studies of exhumed faults and experimentally deformed samples show, however, that the transition from active faulting to creep is not discrete but is more often a zone in which deformation mechanisms and strain localization depend on pressure, temperature, strain rate, grain size, fluid activities, mineralogy, phase transformations, and microstructure (Cole et al., 2007, and reference therein).

By analyzing the 8 months of seismicity pattern preceding the first mainshock of the 2016–2017 Central Italy seismic sequence, we address specific questions of interest concerning how seismic activity along a subhorizontal shear zone placed in the midcrust may contribute in evidencing tectonic loading and how the strain may be partitioned along the overhead crustal faults.

The 1997 Umbria-Marche and 2009 L'Aquila sequences, located to the north and the south of the 2016–2017 sequence, respectively (Figure 1), were both distinguished by foreshocks activity occurred along structural discontinuities in between the main faults (Chiaraluce et al., 2003) and along the main fault plane (Chiaraluce et al., 2011), respectively. In contrast, the crustal volume enclosing the normal faults system responsible for the 2016–2017 seismic sequence displays before the first mainshock a low level of seismic activity ($M_L < 3.3$) mainly occurring along a midcrustal shear zone (depth interval 6–11 km) as well as on portions of the shallower faults that will be reactivated during the sequence (Chiaraluce, Di Stefano et al., 2017). In addition, despite the rather similar geological environment, only the foreshocks pattern of both the 1997

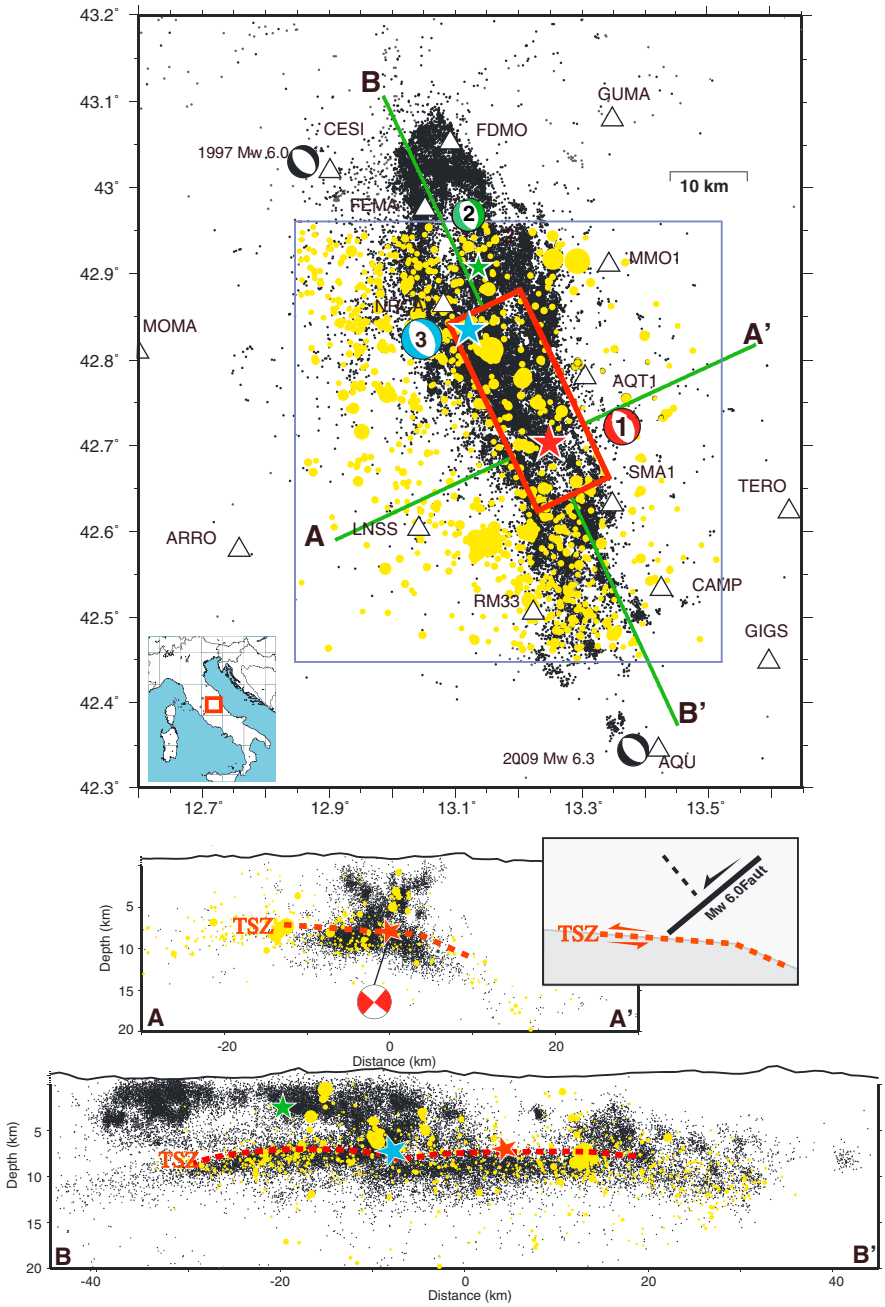

Figure 1. Map view and cross sections of the study area. Template events (yellow dots) and seismic stations (white triangles) locations are superimposed to the aftershocks (black dots) of the 2016–2017 Central Italy seismic sequence (from Chiaraluce, Di Stefano et al., 2017). The focal mechanisms of the three mainshocks of the sequence (red for the 24 August event with M_w6.0, green for the 26 of October M_w5.9 event, and light blue for the 30 of October M_w6.5 shock) are close to the related epicenters (stars). As a reference, we also reported the focal mechanisms of the 1997 Umbria-Marche (M_w6.0) and the 2009 L'Aquila (M_w6.3) mainshocks (black), placed on their epicenters. The red box shows the projection at the surface of the modeled fault plane of the 24 August M_w6.0 (from Tinti et al., 2016). A-A′ cross section reports only the aftershocks occurring within the M_w6.0 source area while in B-B′ all the available events are visible. Within both the cross sections, the template dimension is scaled with the number of repetitions. TSZ = top of shear zone. The inset of cross section A-A′ shows a cartoon of the main discontinuities deduced from the seismicity pattern.

and 2009 sequence gave hints of the involvement of fluids in the earthquake preparatory phase (Lucente et al., 2010; Ripepe et al., 2001; Terakawa et al., 2010).

In this paper, we make use of an improved earthquake catalog we constructed by applying phase match filtering, to describe the seismic activity behavior interpreted as the signature of changes in the tectonic loading along a midcrustal shear zone and on the shallower extensional fault system.

Using both real and simulated earthquake catalogs, many efforts have already been made to characterize the seismicity patterns preceding mainshock occurrence (e.g., Hainzl et al., 2000; Kanamori, 1981; Kawamura, 2006; Mignan, 2014; Wyss & Habermann, 1988) and most of the precursory variations have used definitions based on the presence of relatively anomalous patterns such as quiescence, accelerating seismic release, short-term activation, Mogi doughnut, inward and outward event migration, decelerating seismicity, and *b* value decrease (e.g., Mignan, 2012). These differences are explained by considering physical processes where seismic activity is viewed as a marker of an ongoing preparatory process. In this perspective, an additional pattern, also supported by evidence from laboratory experiments, is the migration of the seismic activity toward the main rupture nucleation point before the mainshock (e.g., Bouchon et al., 2011; Kato et al., 2012), a behavior that can be described by both tectonic loading and epidemic-type aftershock sequence models (e.g., Helmstetter & Sornette, 2003; Ogata, 1988).

Of course, the debate on the rationality and mainly the applicability of the precursory patterns of seismicity is far from being resolved because of the limited number of well-constrained observations and interpretable cases, together with the possibility that data windowing in space and time could largely affect results (e.g., Hardebeck et al., 2008; Zechar & Zhuang, 2010). Thus, the importance of having reliable statistics for an increased number of major earthquakes by improving the detection capabilities of smaller earthquakes is very clear. The seismic activity preceding the onset of the 2016–2017 Central Italy seismic sequence gives us the opportunity to enhance these statistics focusing on the apparent absence of meaningful seismic activity in the 8 months before 24 August 2016, the date of occurrence of the first M_w6.0 mainshock, below and around the activated fault (red box in Figure 1).

2. Data Processing and Catalog Generation

The 2016–2017 seismic sequence, filling a gap in the Apenninic chain between the 1997 Colfiorito and the 2009 L'Aquila earthquakes, has activated so far, an 80 km long normal fault system composed by two main SW dipping fault segments (Figure 1). Three main events occurred with the largest one with M_w6.5 that nucleated on 30 October in the middle and after a M_w6.0 (24 August) to the south and a M_w5.9 (26 October) to the north (Chiaraluce, Di Stefano et al., 2017). One of the main peculiarities of this sequence is that the whole set of high-angle normal faults, confined within the first 8 km of the upper crust, is bounded below by a gently east dipping 2–3 km thick layer in which small events plus a series of larger extensional aftershocks ($\approx M_w$4) occurred (Chiaraluce, Di Stefano et al., 2017). The analysis of the seismic activity in the area, before the sequence onset, showed that this almost horizontal layer was already active (Marzorati et al., 2016), and only small magnitude events ($M_L < 3.3$) took place.

To decrease the completeness magnitude (M_C) of the original catalog (equal to M_C1.4) during the 8 months before the onset of the seismic sequence and thus the final stage of the first mainshock preparatory process, we applied a search for earthquakes that strongly resemble templates (e.g., Kato et al., 2012; Peng & Zhao, 2009; Shelly et al., 2007; Yang et al., 2009; Zhang & Wen, 2015). We selected as templates 1,028 earthquakes (yellow events in Figure 1) from the catalog obtained by Chiaraluce, Di Stefano et al. (2017). These templates are located within 40 km of distance from the first M_w6.0 mainshock and occurred from 1 January to 24 August 2016.

Hypocenter locations and uncertainties of the starting 1,028 events with $0.1 < M_L < 3.3$ are estimated with a 1-D velocity model (Carannante et al., 2013) plus station correction, exploited by a nonlinear inversion code (NonLinLoc; Lomax et al., 2009). The selection of the templates is based on waveform quality and location accuracy rejecting events with formal horizontal/vertical errors greater than 1 and 3 km, respectively, and located with a number of phases less than 10. Horizontal/vertical errors, number of phases, azimuthal gaps, and depths of the 1,028 templates used are shown in Figure S1 in the supporting information.

Cross correlations of daily three-component continuous waveforms sampled at 20 Hz with 1,028 templates are performed by using PyMPA a Python-based phase match filtering (Vuan et al., 2017) in the frequency range from 2 to 5 Hz. Templates are trimmed using a 5 s data window, starting 2.5 s before the theoretical *S* wave arrival. Arrival times are computed using the ObsPy port (Krischer et al., 2015) of the Java TauP Toolkit routines (Crotwell et al., 1999). Seismic data are collected from 17 stations of the national seismic network (white triangles in Figure 1) located in a radius of about 50 km from the investigated fault (red box in Figure 1; from Tinti et al., 2016). The correlograms are evaluated as a function of time, shifting sample by sample the template event window through the continuous waveforms. The threshold, defined after a visual inspection of detected events, is set at 15 times the median absolute deviation of the stacked correlograms. The magnitude of the detected event, as in Peng and Zhao (2009), is calculated as the median value of the maximum amplitude ratios for all channels between the template and detected events, assuming that a tenfold increase in amplitude corresponds to a one unit increase in magnitude. We found many events that are correlated to more than one template in a narrow time window. Time windows of 6 s are selected, and within each one, the template for which the normalized correlation coefficient is the greatest is taken for determining the event location and magnitude (e.g., Kato et al., 2012). By using restrictive criteria on detection threshold, the number of channels considered, and cross-correlation mean values, we found, before the 24 August mainshock, 1,816 new events (e.g., undetected by previous analysis; Figure S2), plus 266 early aftershocks occurred in the first 48 h of the seismic sequence. New detections have smaller magnitudes than the templates, and they increase by about 3 times the size of the starting catalog allowing a substantial decrease of M_C in the augmented catalog from M_L1.4 to less than M_L1.0. It is worth noting that M_C does not vary significantly with time (e.g., during the 8 months preceding the mainshock; Figure S3), implying that the features we are going to identify and discuss by means of the new catalog do not depend on the templates selection.

3. Seismicity Pattern

The vast majority of the 2,844 earthquakes in the catalog, composed by the 1,028 templates and the 1,816 new detections, are located along the midcrustal shear zone consisting of a plane gently dipping to the east and bounding at depth, from 6 km to 11 km, the fault system (yellow events in the cross sections of Figure 1). This shear zone (SZ) highlighted by the seismic activity before and after the onset of the seismic sequence has a lateral extension perpendicular to the chain of about 30 km (cross-section A-A′ in Figure 1) and more than double that along the strike fault extension. Following Chiaraluce, Barchi et al. (2017), we interpret this seismic layer as located directly above (approximately 2 km) the top of the "brittle-ductile" layer modeled for a sector cutting the Apenninic chain 40 km to the north of the cross-section line (A-A′) in Figure 1.

In Figure 2 we compare the presequence seismic activity occurring above and within the SZ for different volumes. We define the earthquakes nucleating within the SZ as the ones that occurred below the top of the shear zone (TSZ in Figure 1). We defined polygons assuming as a reference the projection of the box representing the source of the M_w6.0 fault (Tinti et al., 2016; red volume in Figure 2e). Since TSZ is located at variable crustal depths in the region, we use indications from relocated aftershocks for separating seismicity occurring below TSZ (dashed lines in Figure 2; thus within the SZ) or above it (solid line in Figure 2). The definition of TSZ at variable depths (6–8 km) is possible because of the presence of a thin layer (~1 km) having reduced seismicity. This thin layer separates the shallow extensional fault system activated during the 2016 sequence from the underlying shear zone with very high seismicity (Figure 1).

We observe that seismicity within the SZ is more widespread than that at shallow depth around the main normal faults. Especially in the southern sectors (volumes *g* and *h* in Figure 2) in a 400 km^2 area, most of the seismicity is located at a depth between 7 and 11 km. The seismicity distribution at depth changes in the crustal volumes containing the M_w6.0 fault segment and in its footwall (Figures 2e and 2f). In the main source volume (Figure 2e) we observe shallower seismicity increasing from mid-April and becoming predominant from midend of June when there were fewer events at depth along the SZ. In the same period in the footwall volume (Figure 2f) the seismicity at shallow depth, which is always more abundant than the deeper one, shows an additional minor increase. The seismicity pattern we observe all around the M_w6.0 source volume may be an indication of partitioning of the strain between the upper and middle to lower crust along the SZ.

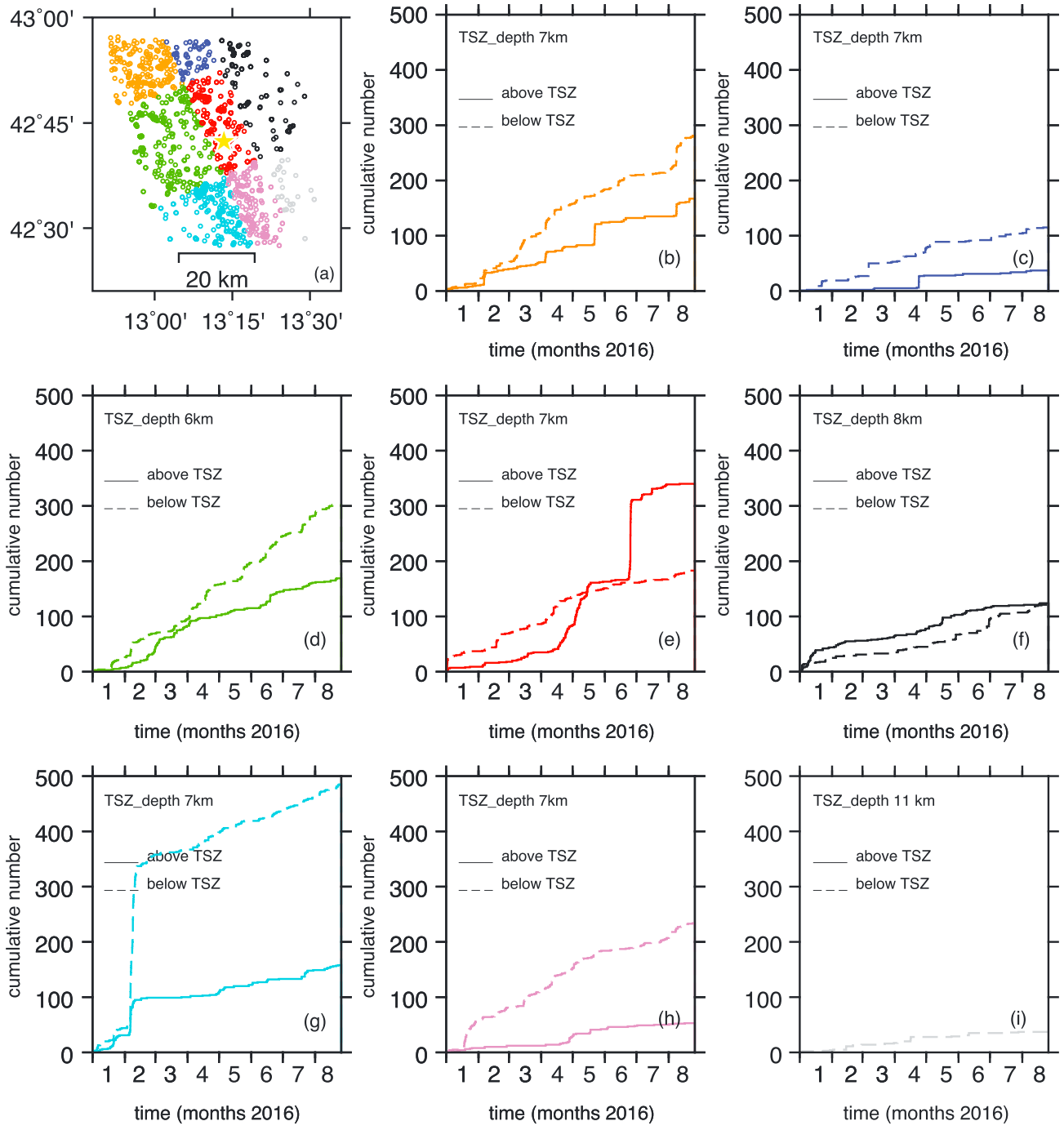

Figure 2. (a) Map view of the presequence seismic events. The color coding is based on the occurrence within distinct crustal volumes respect to the central one containing the M_w6.0 fault plane (see text for further explanation). (b–i) Cumulative number of earthquakes above (solid line) and below (dashed line) TSZ defined based on the depth of the events, for different subvolumes.

Figure 3 shows the location of the seismicity in map view (Figures 3a and 3b) and the space-time distribution of the events along the fault strike of the 24 August M_w6.0 (Figures 3c and 3d) in the shallower crust and along the SZ. During the 8 months, the seismicity along the SZ (Figure 3b) is diffused over a wider area than the shallow seismicity (Figure 3a).

Earthquakes recurrent over time are also shown in Figures 3a and 3b; the larger the circle size, the higher is the number of detected earthquakes by the same template. East and south of the main fault volume,

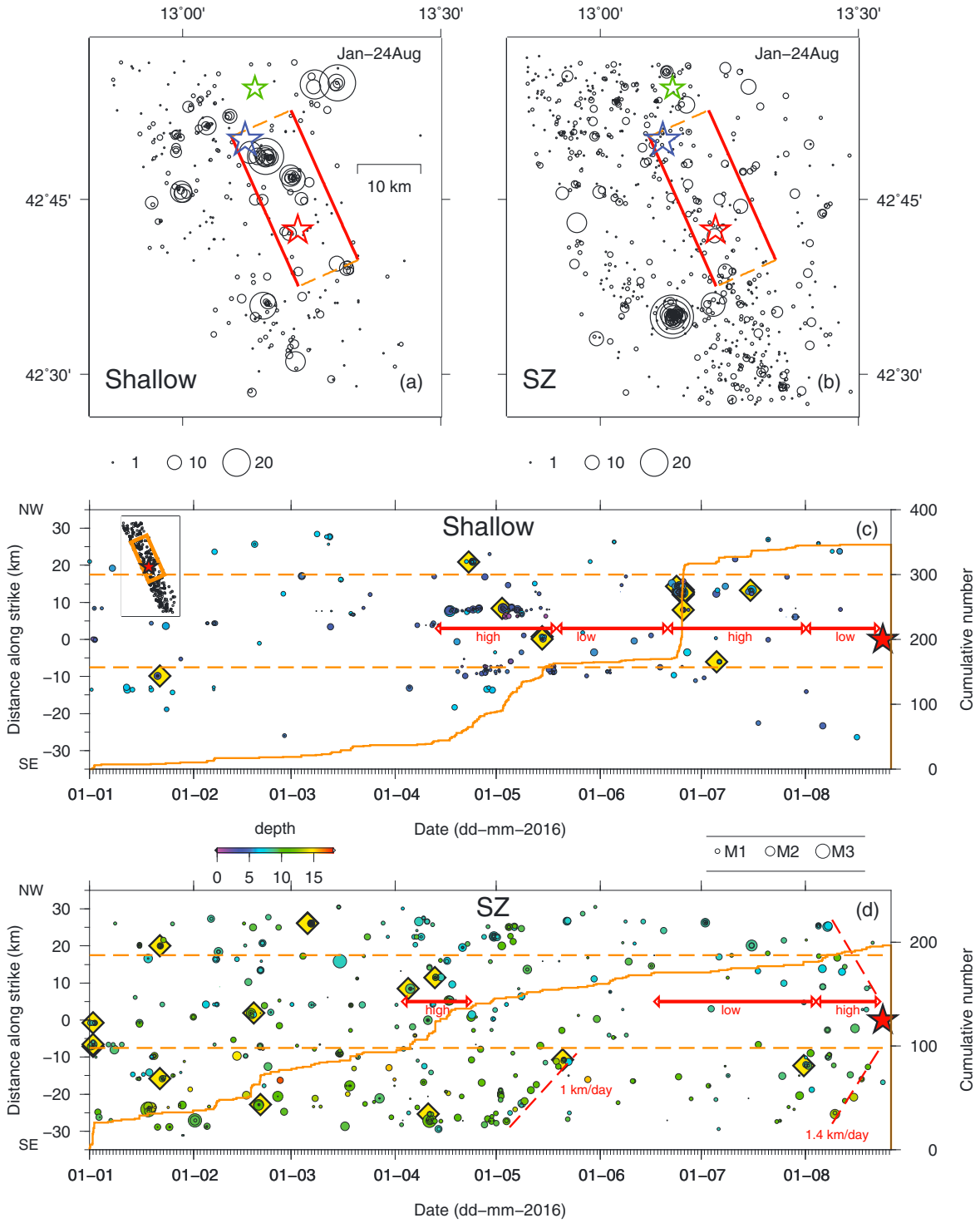

Figure 3. Map view of the (a) shallow and (b) deeper seismicity (occurring respectively above and along the gently dipping shear zone, SZ) detected in the epicentral area of the Central Italy sequence from 1 January 2016 to 24 August 2016, date of occurrence of the M_w6.0 earthquake. The red, green, and blue stars correspond to the epicenters of the three mainshocks of 24 August (M_w6.0), 26 October (M_w5.9), and 30 October (M_w6.5), respectively. The red box represents the projection at the surface of the 24 August M_w6.0 earthquake (from Tinti et al., 2016). White circles size is scaled with the number of repetitions over the 8 months (see legend below Figure 3a, b). Space-time diagrams are drawn along NW trending direction of the (c) shallow and (d) deeper relocated events. The selected stripe has approximately 10 km of lateral extension along strike and includes events shown in Figures 2c, 2e, and 2h. Distance taken along the fault strike (156° oriented cross section): 0 distance corresponds to the hypocenter of the 24 August M_w6.0 mainshock (red star); positive and negative distances on the bottom panel represent the seismicity north and south of the mainshock, respectively. The cumulative number of events (orange plain line) within the main fault volume is also shown as in Figure 2e. Orange dotted lines mark the northern and southern limits of the M_w6.0 fault plane. Yellow diamonds represent recurrent detections (≥ 5) in a 48 h sliding time window.

the recurrent shallow seismicity is almost absent (Figure 3a) while diffuse events are found at depth (Figure 3b). Along the SZ, seismicity and recurrent events occur instead persistently south and north of the main fault, while in the west and east sectors (hanging wall and footwall, respectively) there are fewer earthquakes.

The M_w6.0 main fault volume mainly exhibits shallow seismicity (Figure 3a) with earthquakes repeating close to the 24 August M_w6.0 and 30 October M_w6.5 nucleation points. The events also occur at the northern and southern edges of the fault plane. Fewer recurrent earthquakes are found along the SZ below the main fault volume.

Monthly shallow and deep seismicity detected in the area of the 2016 Central Italy sequence before 24 August M_w6.0 earthquake is shown in Figure S4. The quasi-repeaters within the SZ are mostly recurring at the same critical points from January to April 2016 (see Figure S4, b1–b4), while the productivity of shallow events becomes evident from April to July 2016 (see Figure S4, a4–a7). In July and August (see Figures S4, a7 and a8 and S2, b7 and b8) we observe a considerable reduction of the seismic activity within the main fault.

The space-time diagrams (Figures 3c and 3d) confirm that events at depth are more frequent, especially in the northern and southern volumes along strike. Shallow earthquakes mostly concentrate within the main fault plane along shorter distances from the M_w6.0 hypocenter (± 10 km; see Figure 3c). The gradual increase of the events along the SZ and the main fault plane in the first months of 2016 is characterized by an acceleration of the seismic release at the beginning of April (Figure 3d) that seems to trigger an ~ 10 day delayed increase in the shallow seismicity (Figure 3c). Detections associated with the same template and characterized by a number of occurrences $\geq$5 in a 48 h time window are also shown in Figures 3c and 3d (yellow diamonds). Recurrent events over time are found within high-rate seismicity time windows.

From the beginning of May, we observe a migration at about 1 km/d toward the fault plane. Few shallow events are detected within the main fault volume from mid-May to about 20 June. In Figure 3c, in the same volume, we also observe some phases of increasing seismic rate (high) and relaxation (low) for the shallow earthquakes that seem time shifted in comparison with those along the SZ (see Figure 3d). These variations of the seismic rate within the main fault volume are also evident in the cumulative number of earthquakes shown in Figures 3c and 3d. From mid-June to the beginning of August we record an apparent quiescence or relaxation at depth (Figure 3d) that is synchronous with a relatively sudden increasing rate of shallow seismicity close to the northern end of the main fault plane. An increased rate at depth together with a migration episode (faster than before: 1.4 km/d) is observed in August, starting about 1 month before the mainshock. This migration, better constrained in the southern sector (Figure 3d), points to the nucleation of the M_w6.0, while no corresponding shallower seismic activity is recorded.

Thus, evaluating the space-time variation in the rate of occurrence of the seismic events identifies two main episodes of inward seismicity migration. We verified the influence of M_C in the inward migration pattern recognition, and we observe that seismicity patterns remain consistent independently if we take into account all the augmented catalog of events or only those above M_C. These migration episodes, marked in Figure 3d, anticipate two time windows when we observe a lower rate of events. In addition to this, the measured migration velocities of approximately 1 km/d are critical for this sector of the Apennines. About 0.5–1 km/d as an apparent migration velocity value was observed in the L'Aquila foreshock sequence 2 months before the 2009 mainshock (e.g., Sugan et al., 2014) and 1 km/d characterize the sequence migration in the Umbria-Marche 1997 (Antonioli et al., 2005).

4. Discussion

The preparatory phase of the 24 August 2016 M_w6.0 earthquake in Central Italy is characterized by some peculiarities in the seismicity pattern evolution that could remain hidden if not analyzed in detail by using phase match filtering or similar methods. We identify the following features characterizing the system in an area of 50 km along fault strike and 30 km across the system: (1) presence of diffuse seismicity at depths ranging from 6 to 11 km along a subhorizontal interface (SZ) in the 8 month period preceding the seismic sequence onset; (2) shallow seismicity (0–6 km), located on the dipping planes of normal faults, recurrent over time and space and almost absent south and east of the main fault volume; (3) seismic rate along

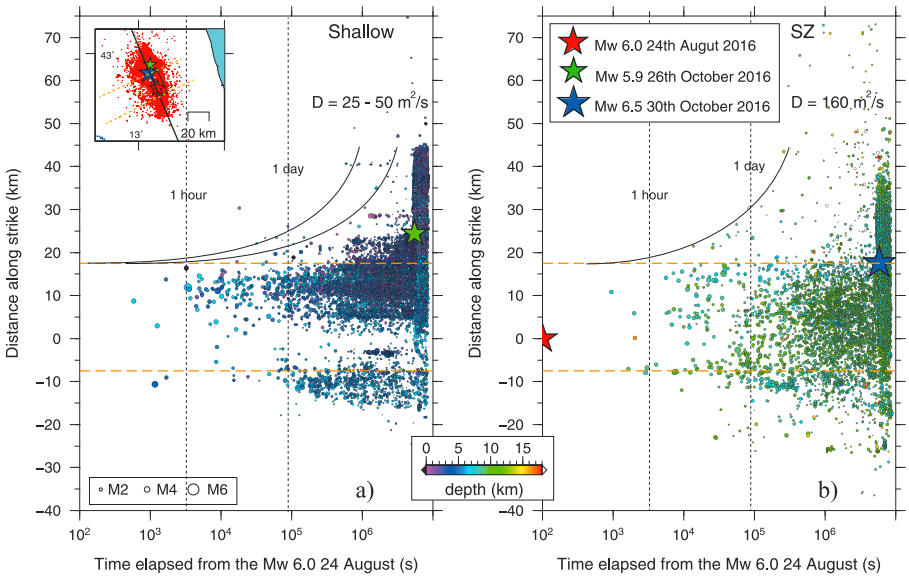

Figure 4. Spatial and temporal evolution of the seismic sequence between the 24 August M_w6.0 and the 30 October M_w6.5 earthquakes. The catalog of the early aftershocks of Chiaraluce, Di Stefano et al. (2017) has been enhanced by adding the 266 newly detected events occurred in the first 48 h after the M_w6.0 mainshock. (a) Shallow (blue events) and (b) deeper (green events) earthquakes. Dashed lines (orange) define the along-strike extension of the M_w6.0 fault plane. Black dashed lines indicate a linear fit for the off-fault aftershocks migration used to compute the diffusion coefficient (D).

the SZ, all around the 24 August fault area, is higher than that at shallower depths, while within the main fault volume, shallow earthquakes prevail. This evidence suggests that earthquakes (e.g., slip), occurring along the low-angle SZ and around the source area of the first mainshock, increased the stress at the main fault edges allowing the growth of the fractures pattern with a consequent unlocking of normal fault portions located above (see the simplified scheme of the A-A′ cross section in Figure 1). Such fault unzipping seems also modulated over time by the seismicity migration episodes along the SZ observed in Figure 3d. The validation of the kinematic compatibility (e.g., by moment tensor for small magnitude earthquakes) of this mechanism is behind the scope of this paper deserving a dedicated analysis.

From these observations, we argue that changes in the seismicity pattern along the SZ could be related to a tectonic loading process taking place along the midcrustal SZ, varying with time and partitioning the strain on the shallower crust. To further investigate the different behavior of the SZ and the shallower faults in accommodating the coseismic strain, we analyzed the space-time distribution of the early aftershocks including the 266 new earthquakes we detected in the 2 days immediately following the 24 August M_w6.0 mainshock. It is important to note that these 266 additional aftershocks, we retrieved with the template matching technique and that are added to the available catalog (574 events from Chiaraluce, Di Stefano et al., 2017), are detected by using the same set of 1,028 templates recorded before the mainshock. Figures 4a and 4b show that the early aftershocks immediately propagated in an area considerably larger than the size itself of the activated fault. We observe in fact a clear off-fault expansion of the aftershocks toward portions located both north and south of the source. We model this early aftershock migration, which occurred soon after (48 h) the mainshock, looking for diffusion processes recovered by analyzing the evolution in space and time of the shallower (Figure 4a) and the deeper (along SZ) seismicity (Figure 4b). We apply Darcy's law proposed by Shapiro et al. (2003) defining a triggering front $r = (4\pi Dt)^{0.5}$ related to the time (t) and the scalar diffusivity (D). We end up with two very different speeds corresponding to highly different diffusion coefficient values: 25–50 m^2/s for the shallow events against the 160 m^2/s for the events migrating along the SZ. Even if the D value estimated for the shallow seismicity is less robust because of the limited number of earthquakes considered, here the relevant aspect is the large discrepancy between the two measured values. Assuming that the value observed for the expansion of shallow seismicity is correct, it could certainly be explained by an aftershock model derived from the rate and state frictional law (Dieterich, 1994). In addition to this, D = 25–50 m^2/s is a value consistent with the values inferred from the 1997 Colfiorito and

2009 L'Aquila neighboring sequences (see Chiaraluce (2012) for a review) where a role for overpressurized fluids is proposed.

On the contrary, the very high off-fault diffusivity value observed along the SZ requests a different explanation. In general, early aftershocks off-fault expansion can be due to static stress changes, viscoelastic relaxation, fluid diffusion, dynamic triggering, or afterslip. The aftershock pattern, directed especially north-northeast and south, cannot be due to static stress changes. In fact, as shown in Convertito et al. (2017), Coulomb stress change is positive in the aftershock area, but most of the early events are at distances where the stress change is close to zero. We can also exclude a viscoelastic relaxation for the longer times needed to develop (we observe a migration of ~10 km in 24 h) and fluid influence for the very high diffusivity values we measured at depth. We could think of an induced dynamic triggering effect due to source directivity. However, the 24 August mainshock slip distribution is bilateral (see Tinti et al., 2016) with no meaningful slip at the fault bottom. In case of prevailing dynamic triggering, we expected to measure higher diffusivity values in the shallower crust. Based on these observations, one of the remaining possible explanations for the observed off-fault migration is the occurrence of an afterslip episode inducing small events, along with the SZ. In this framework, the apparent high-speed velocity expansion (approximately 8–10 km/d as shown in Figure 4) is consistent with previous studies (5–30 km/d) investigating early aftershocks to identify afterslip (Chang et al., 2007; Kato et al., 2016; Kato & Obara, 2014; Lengliné et al., 2012; Meng & Peng, 2016; Peng & Zhao, 2009; Tang et al., 2014; Yao et al., 2017). As an additional and indirect validation for the afterslip occurrence, we evaluated the presence and behavior of the quasi-repeaters (cross-correlation values between 0.65 and 0.8) and repeaters ($>$ 0.8) recorded by near-fault stations (Figure S5) during the first 48 h after the mainshock. We observed quasi-repeaters and repeaters to occur below the main fault plane, in the footwall and outside (north-south) the fault area. The evidence of this off-fault expansion corroborates our hypothesis suggesting that afterslip may be the driving force triggering repeaters at similar critical points and seismicity migration with high D values along the SZ. These features mimicking the propagation of an aseismic slip transient also indicate a certain degree of decoupling between the shallow crust and the underlying structure (SZ) as well as the signature of loading rate variation/modulation continuing after the M_w6.0 earthquake.

5. Conclusions

Hidden features characterizing the microseismicity pattern in the 8 months before the 2016 August M_w6.0 mainshock are observed by increasing the number of detected events. We focus the investigation on the modulations of earthquakes occurrence along a midcrustal shear zone, causing tectonic load variations and a gradual unlocking of the overlaying normal faults. Asynchrony is observed in the occurrence of seismic events nucleating along this deeper interface compared to the ones occurring on fault portions embedded in the shallower upper crustal volume, with the former anticipating the latter. We interpret this behavior as the signature of strain partitioning between the middle and upper crust. An increase in the rate of seismic release at depth in areas close to the main fault volume corresponds to a delayed increase in events in the upper portion. Other peculiarities of the seismic sequence suggest a decoupling between a brittle upper crust and a possibly aseismic lower crust active along this midcrustal shear zone.

Seismicity occurring along the SZ has a broader spatial extension than that in the shallower crust. Within the deeper layer, we also observe seismicity migrating along strike toward the first M_w6.0 mainshock nucleation point at relatively low speed (1–1.4 km/d) in May 2016 and 20 days before the M_w6.0 earthquake. These episodes are followed by an apparent quiescence in June and July 2016 within the main fault area.

All these observations are indicative of a preparatory phase that can be related to a tectonic loading process leading to suppose aseismic slip phenomenon at depth, whose seismic activity along the low-angle shear zone, acting as detachment, could be the brittle signature. Variations in the tectonic loading may have contributed to increasing the stress in a broad area with a growth of the fracture pattern in the fault zone prone to rupture. The decoupling between the shallow crust and the underlying structure is also evident from the extension of the aftershock area immediately after the M_w6.0 earthquake. We observe very high values of the diffusion coefficient at depth that are interpreted as afterslip induced by the 24 August mainshock, likely contributing to the loading of the 26 October M_w5.9 and 30 October M_w6.5 main fault planes.

Acknowledgments

The data to support this article are available accessing the European Integrated Data Archive managed by Istituto Nazionale di Geofisica e Vulcanologia (http://eida.rm.ingv.it/). Computations are performed at CINECA in the framework of the HPC-TRES program agreement between OGS and CINECA. This study is in part funded by a joint research project within the executive program of scientific and technological cooperation between Italy and Japan. We thank Aitaro Kato, Bill Ellsworth, Warner Marzocchi and Massimo Cocco for useful comments and suggestions on a preliminary version of the paper. We also thank Giorgio Amati at Cineca for providing the support in computations and Tony Brauer for his comments and the high-quality proofreading of the English. Figures were produced using the Generic Mapping Tools version 5.0 (www.soest.hawaii.edu/gmt; Wessel & Smith, 1991).

References

Antonioli, A., Piccinini, D., Chiaraluce, L., & Cocco, M. (2005). Fluid flow and seismicity pattern: Evidence from the 1997 Umbria-Marche (central Italy) seismic sequence. *Geophysical Research Letters*, *32*, L10311. https://doi.org/10.1029/2004GL022256

Bouchon, M., Karabulut, H., Aktar, M., Ozalabey, S., Schmittbuhl, J., & Bouin, M. P. (2011). Extended nucleation of the 1999 M_w 7.6 Izmit earthquake. *Science*, *331*, 877–880. https://doi.org/10.1126/science.1197341

Brace, W. F., & Kohlstedt, D. L. (1980). Limits on lithospheric stress imposed by laboratory experiments. *Journal of Geophysical Research*, *85*(B11), 6248–6252. https://doi.org/10.1029/JB085iB11p06248

Byerlee, D. J. (1978). Friction of rocks. *Pure and Applied Geophysics*, *116*, 615–626.

Carannante, S., Monachesi, G., Cattaneo, M., Amato, A., & Chiarabba, C. (2013). Deep structure and tectonics of the northern-central Apennines as seen by regional-scale tomography and 3-D located earthquakes. *Journal of Geophysical Research: Solid Earth*, *118*, 5391–5403. https://doi.org/10.1002/jgrb.50371

Chang, C. H., Wu, Y.-M., Zhao, L., & Wu, F. T. (2007). Aftershocks of the 1999 Chi-Chi, Taiwan, earthquake: The first hour. *Bulletin of the Seismological Society of America*, *97*, 1245–1258. https://doi.org/10.1785/0120060184

Chiaraluce, L. (2012). Unravelling the complexity of Apenninic extensional fault systems: A review of the 2009 L'Aquila earthquake (Central Apennines, Italy). *Journal of Structural Geology*, *42*, 2–18. https://doi.org/10.1016/j.jsg.2012.06.007

Chiaraluce, L., Ellsworth, W. L., Chiarabba, C., & Cocco, M. (2003). Imaging the complexity of an active normal fault system: The 1997 Colfiorito (cental Italy) case study. *Journal of Geophysical Research*, *108*(B6), 2294. https://doi.org/10.1029/2002JB002166

Chiaraluce, L., Valoroso, L., Piccinini, D., Di Stefano, R., & De Gori, P. (2011). The anatomy of the 2009 L'Aquila normal fault system (central Italy) imaged by high resolution foreshock and aftershock locations. *Journal of Geophysical Research*, *116*, B12311. https://doi.org/10.1029/2011JB008352

Chiaraluce, L., Di Stefano, R., Tinti, E., Scognamiglio, L., Michele, M., Casarotti, E., … Marzorati, S. (2017). The 2016 Central Italy seismic sequence: A first look at the mainshocks, aftershocks, and source models. *Seismological Research Letters*, *88*(3), 757–771. https://doi.org/10.1785/0220160221

Chiaraluce, L., Barchi, M. R., Carannante, S., Collettini, C., Mirabella, F., Pauselli, C., & Valoroso, L. (2017). The role of rheology, crustal structures and lithology in the seismicity distribution of the northern Apennines. *Tectonophysics*, *694*, 280–291. https://doi.org/10.1016/j.tecto.2016.11.011

Cole, J., Hacker, B., Ratschbacher, L., Dolan, J., Seward, G., Frost, E., & Frank, W. (2007). Localized ductile shear below the seismogenic zone: Structural analysis of an exhumed strike-slip fault, Austrian Alps. *Journal of Geophysical Research*, *112*, B12304. https://doi.org/10.1029/2007JB004975

Convertito, V., De Matteis, R., & Pino, N. A. (2017). Evidence for static and dynamic triggering of seismicity following the 24 August 2016, M_w = 6.0, Amatrice (Central Italy) earthquake. *Pageoph*, *174*(10), 3663–3672. https://doi.org/10.1007/s00024-017-1559-1

Crotwell, H. P., Owens, T. J., & Ritsema, J. (1999). The TauP toolkit: Flexible seismic travel-time and ray-path utilities. *Seismological Research Letters*, *70*(2), 154–160. https://doi.org/10.1785/gssrl.70.2.154

Dieterich, J. (1994). A constitutive law for rate of earthquake production and its application to earthquake clustering. *Journal of Geophysical Research*, *99*(B2), 2601–2618. https://doi.org/10.1029/93JB02581

Hainzl, S., Zoller, G., Kurths, J., & Zschau, J. (2000). Seismic quiescence as an indicator for large earthquakes in a system of self-organized criticality. *Geophysical Research Letters*, *27*(5), 597–600. https://doi.org/10.1029/1999GL011000

Hardebeck, J. L., Felzer, K., & Michael, A. J. (2008). Improved tests reveal that the accelerating moment release hypothesis is statistically insignificant. *Journal of Geophysical Research*, *113*, B08310. https://doi.org/10.1029/2007JB005410

Helmstetter, A., & Sornette, D. (2003). Foreshocks explained by cascades of triggered seismicity. *Journal of Geophysical Research*, *108*(B10), 2457. https://doi.org/10.1029/2003JB002409

Kanamori, H. (1981). The nature of seismicity patterns before large earthquakes. In W. Simpson & G. Richards (Eds.), *Earthquake prediction: An international review*, (pp. 1–19). Washington, DC: American Geophysical Union.

Kato, A., & Obara, K. (2014). Step-like migration of early aftershocks following the 2007 M_w 6.7 Noto-Hanto earthquake, Japan. *Geophysical Research Letters*, *41*, 3864–3869. https://doi.org/10.1002/2014GL060427

Kato, A., Obara, K., Igarashi, T., Tsuruoka, H., Nakagawa, S., & Hirata, N. (2012). Propagation of slow slip leading up to the 2011 M_w 9.0 Tohoku-Oki earthquake. *Science*, *335*, 705–708. https://doi.org/10.1126/science.1215141

Kato, A., Fukuda, J., Nakagawa, S., & Obara, K. (2016). Foreshock migration preceding the 2016 M_w 7.0 Kumamoto earthquake, Japan. *Geophysical Research Letters*, *43*, 8945–8953. https://doi.org/10.1002/2016GL070079

Kawamura, H. (2006). Spatiotemporal correlations of earthquakes. In P. Bhattacharyya & B. K. Chakrabarti (Eds.), *Lecture notes in physics, 705, modelling critical and catastrophic phenomena in geoscience* (pp. 223–257). Berlin: Springer. https://doi.org/10.1007/3-540-35375-5_9

Krischer, L., Megies, T., Barsch, R., Beyreuther, M., Lecocq, T., Caudron, C., & Wassermann, J. (2015). ObsPy: A bridge for seismology into the scientific Python ecosystem. *Computational Science & Discovery*, *8*(1), 014003. https://doi.org/10.1088/1749-4699/8/1/014003

Lengliné, O., Enescu, B., Peng, Z., & Shiomi, K. (2012). Decay and expansion of the early aftershock activity following the 2011, M_w9.0 Tohoku earthquake. *Geophysical Research Letters*, *39*, L18309. https://doi.org/10.1029/2012GL052797

Lomax, A., Michelini, A., & Curtis, A. (2009). Earthquake location, direct, global-search methods. In *Complexity in encyclopedia of complexity and system science, Part 5* (pp. 2449–2473). New York: Springer. https://doi.org/10.1007/978-0-387-30440-3, www.springerlink.com

Lucente, F. P., De Gori, P., Margheriti, L., Piccinini, D., Di Bona, M., Chiarabba, C., & Agostinetti, N. P. (2010). Temporal variation of seismic velocity and anisotropy before the 2009 M_w 6.3 L'Aquila earthquake. Italy. *Geology*, *38*, 1015–1018. https://doi.org/10.1130/G31463.1

Marzorati, S., Cattaneo, M., Frapiccini, M., Monachesi, G., & Ladina, C. (2016). Recent seismicity before the 24 August 2016 M_w 6.0 central Italy earthquake as recorded by the ReSIICO seismic network. *Annals of Geophysics*, *59*, 1–12. https://doi.org/10.4401/ag-7191

Meng, X., & Peng, Z. (2016). Increasing lengths of aftershock zones with depths of moderate-size earthquakes on the San Jacinto Fault suggests triggering of deep creep in the middle crust. *Geophysical Journal International*, *204*(1), 250–261. https://doi.org/10.1093/gji/ggv445

Mignan, A. (2012). Seismicity precursors to large earthquakes unified in a stress accumulation framework. *Geophysical Research Letters*, *39*, L21308.

Mignan, A. (2014). The debate on the prognostic value of earthquake foreshocks: A meta-analysis. *Scientific Reports*, *4*, 4099. https://doi.org/10.1038/srep04099

Ogata, Y. (1988). Statistical models for earthquake occurrences and residual analysis forpoint processes. *Journal of the American Statistical Association*, *83*(401), 9–27. https://doi.org/10.1080/01621459.1988.10478560

Peng, Z., & Zhao, P. (2009). Migration of early aftershocks following the 2004 Parkfield earthquake. *Nature Geoscience*, *2*, 877–881. https://doi.org/10.1038/ngeo697

Ripepe, M., Piccinini, D., & Chiaraluce, L. (2001). Foreshock sequence of September 26th, 1997 Umbria-Marche earthquakes. *Journal of Seismology*, *4*(4), 387–399.

Shapiro, S. A., Patzig, R., Rothert, E., & Rindschwentner, J. (2003). Triggering of seismicity by pore pressure perturbations: Permeability related signature of the phenomenon. *Pure and Applied Geophysics*, *160*(5), 1051–1066. https://doi.org/10.1007/PL00012560

Shelly, D. R., Beroza, G. C., & Ide, S. (2007). Non-volcanic tremor and low-frequency earthquake swarms. *Nature*, *446*, 305–307. https://doi.org/10.1038/nature05666

Sibson, R. H. (1977). Fault rocks and fault mechanisms. *Journal of the Geological Society of London*, *133*(3), 191–213. https://doi.org/10.1144/gsjgs.133.3.0191

Sibson, R. H. (1982). Fault zone models, heat flow, and the depth distribution of earthquakes in the continental crust of the United States. *Bulletin of the Seismological Society of America*, *72*(1), 151–163.

Sugan, M., Kato, A., Miyake, H., Nakagawa, S., & Vuan, A. (2014). The preparatory phase of the 2009 M_w 6.3 L'Aquila earthquake by improving the detection capability of low-magnitude foreshocks. *Geophysical Research Letters*, *41*, 6137–6144. https://doi.org/10.1002/2014GL061199

Tang, C.-C., Lin, C.-H., & Peng, Z. (2014). Spatial-temporal evolution of early aftershocks following the 2010 M_L6.4 Jiashian earthquake in southern Taiwan. *Geophysical Journal International*, *199*(3), 1772–1783. https://doi.org/10.1093/gji/ggu361

Terakawa, T., Zoporowski, A., Galvan, B., & Miller, S. (2010). High-pressure fluid at hypocentral depths in the L'Aquila region inferred from earthquake focal mechanisms. *Geology*, *38*, 995–998. https://doi.org/10.1130/G31457.1

Tinti, E., Scognamiglio, L., Michelini, A., & Cocco, M. (2016). Slip heterogeneity and directivity of the M_L 6.0, 2016, Amatrice earthquake estimated with rapid finite fault inversion. *Geophysical Research Letters*, *43*, 10,745–10,752. https://doi.org/10.1002/2016GL071263

Vuan, A., Sugan, M., Chiaraluce, L., & Di Stefano, R. (2017). Improving the detection of low-magnitude seismicity preceding the M_w 6.3 L'Aquila earthquake: Development of a scalable code based on the cross-correlation of template earthquakes. *Bulletin of the Seismological Society of America*. https://doi.org/10.1785/0120170106

Wessel, P., & Smith, W. H. F. (1991). Free software helps map and display data. *Eos, Transactions of the American Geophysical Union*, *72*(441), 1991.

Wiemer, S., & Wyss, W. (2000). Minimum magnitude of completeness in earthquake catalogues: Examples from Alaska, the western United States, and Japan. *Bulletin of the Seismological Society of America*, *90*(4), 859–869. https://doi.org/10.1785/0119990114

Woessner, J., & Wiemer, S. (2005). Assessing the quality of earthquake catalogues: Estimating the magnitude of completeness and its uncertainty. *Bulletin of the Seismological Society of America*, *95*, 684–698. https://doi.org/10.1785/012040007

Wyss, M., & Habermann, R. E. (1988). Precursory seismic quiescence. *Pure and Applied Geophysics*, *126*(2-4), 319–332. https://doi.org/10.1007/BF00879001

Yang, H., Zhu, L., & Chu, R. (2009). Fault-plane determination of the 18 April 2008 Mount Carmel, Illinois, earthquake by detecting and relocating aftershocks. *Bulletin of the Seismological Society of America*, *99*, 3413–3420. https://doi.org/10.1785/0120090038

Yao, D., Walter, J. I., Meng, X., Hobbs, T. E., Peng, Z., Newman, A. V., … Protti, M. (2017). Detailed spatio-temporal evolution of microseismicity and repeating earthquakes following the 2012 M_w 7.6 Nicoya earthquake. *Journal of Geophysical Research: Solid Earth*, *122*, 524–542. https://doi.org/10.1002/2016JB013632

Zechar, J. D., & Zhuang, J. (2010). Risk and return: Evaluating reverse tracing of precursors earthquake predictions. *Geophysical Journal International*, *182*, 1319–1326. https://doi.org/10.1111/j.1365-246X.2010.04666.x

Zhang, M., & Wen, L. (2015). An effective method for small event detection: Match and locate (M&L). *Geophysical Journal International*, *200*(3), 1523–1537. https://doi.org/10.1093/gji/ggu466